

The stellar (n, γ) cross section of ^{62}Ni

H. Nassar¹, M. Paul^{1*}, I. Ahmad², D. Berkovits³, M. Bettan³, P. Collon⁴, S. Dababneh⁵, S. Ghelberg¹, J.P. Greene², A. Heger⁶, M. Heil⁵, D.J. Henderson², C.L. Jiang², F. Käppeler⁵, H. Koivisto⁷, S. O'Brien⁴, R.C. Pardo², N. Patronis⁸, T. Pennington^{2†}, R. Plag⁵, K.E. Rehm², R. Reifarth⁶, R. Scott², S. Sinha², X. Tang², R. Vondrasek²

¹ *Racah Institute of Physics, Hebrew University, Jerusalem, Israel, 91904*

² *Argonne National Laboratory, Argonne, IL 60439, USA*

³ *Soreq Nuclear Research Center, Yavne, Israel 81800*

⁴ *Physics Department, University of Notre Dame, Notre Dame, IN 46556, USA*

⁵ *Forschungszentrum Karlsruhe Institut für Kernphysik, PF 3640, 76201 Karlsruhe, Germany*

⁶ *Los Alamos National Laboratory, Los Alamos, NM 87545, USA*

⁷ *Department of Physics, University of Jyväskylä, FIN-40351, Finland and*

⁸ *Department of Physics, The University of Ioannina, 45110 Ioannina, Greece*

(Dated: August 14, 2018)

The $^{62}\text{Ni}(n, \gamma)^{63}\text{Ni}(t_{1/2}=100\pm 2 \text{ yrs})$ reaction plays an important role in the control of the flow path of the slow neutron-capture (s -) nucleosynthesis process. We have measured for the first time the total cross section of this reaction for a quasi-Maxwellian ($kT=25 \text{ keV}$) neutron flux. The measurement was performed by fast-neutron activation, combined with accelerator mass spectrometry to detect directly the ^{63}Ni product nuclei. The experimental value of $28.4\pm 2.8 \text{ mb}$, fairly consistent with a recent calculation, affects the calculated net yield of ^{62}Ni itself and the whole distribution of nuclei with $62 < A < 90$ produced by the weak s -process in massive stars.

PACS numbers: 25.40.Lw, 27.50.+e, 97.10.Tk, 82.80.Ms, 29.40.Cs

The quest for experimentally determined cross sections of stellar nucleosynthesis reactions becomes more focused with the refinement of theoretical models and calculation techniques. Above $A=60$ and except for rare cases, nuclei are created by captures of free neutrons in two main mechanisms, the slow (s -)process and rapid (r -)process [1]. The path of the weak s -process component, related to helium burning in massive stars of 10 to 25 M_{\odot} (M_{\odot} denotes one solar mass)[2], starts with the major ^{56}Fe seed nucleus and, proceeding through the neutron-rich Ni region, dominates the synthesis of nuclei with masses between 60 and 90. The particular importance of the cross section of neutron capture reactions in the Ni region has been emphasized by Rauscher *et al.* [3] who suggest that inaccurate cross section values may be responsible for the overestimate of neutron-rich Ni isotope abundances (compared to solar abundances) in nucleosynthesis calculations. The role of the $^{62}\text{Ni}(n, \gamma)^{63}\text{Ni}$ reaction is critical in this respect because it affects the entire weak s -process flow starting from ^{56}Fe . In that regime, the neutron exposure is not strong enough to drive the system to the so-called local equilibrium and the neutron capture rate of a nucleus such as ^{62}Ni , will affect not only the calculated abundance of this nucleus itself, but also that of all following ones. The experimental information on the $^{62}\text{Ni}(n, \gamma)^{63}\text{Ni}$ reaction cross section at keV energies before this work relied on neutron

time-of-flight (TOF) measurements aimed at determining resonance parameters [4, 5]. The more recent values of the Maxwellian-averaged capture cross section (MACS, see definition in [6]) at $kT=30 \text{ keV}$, evaluated from these data and from the thermal (2200 m/s) neutron-capture cross section [7], are $35.5\pm 4 \text{ mb}$ ([8], [6]) and $12.5\pm 4 \text{ mb}$ [9]. The decrease by a factor of ~ 3 in [9] results from the subtraction of the contribution of a sub-threshold resonance, prior to extrapolation to higher energies. Moreover, as later emphasized in ref.[10], none of these evaluations include a possibly significant direct-capture (DC) component. In ref.[10], the DC s - and p -wave contributions were calculated and added to the resonant component to evaluate the $^{62}\text{Ni}(n, \gamma)^{63}\text{Ni}$ MACS up to $kT=500 \text{ keV}$; the MACS at $kT=30 \text{ keV}$ is estimated as $35\pm 5 \text{ mb}$. We report here the first experimental determination of the total $^{62}\text{Ni}(n, \gamma)^{63}\text{Ni}$ cross section for quasi-Maxwellian neutrons ($kT=25 \text{ keV}$). The measurement was performed by a fast-neutron activation coupled for the first time with accelerator mass spectrometry (AMS). Detection of the decay radiation of the long-lived product $^{63}\text{Ni}(t_{1/2} = 100 \pm 2 \text{ yrs}, \beta^- \text{ endpoint energy of } 66 \text{ keV and no } \gamma)$ is impractical and is replaced in the AMS technique (see [11]) by the counting of ^{63}Ni ions, unambiguously identified after acceleration to several MeV/ u . The MACS $\sigma_V = \langle \sigma v \rangle / v_T$ is extracted from the AMS determination of the isotopic ratio in the activated material, using the integrated neutron flux $\langle \phi t \rangle$ monitored during activation.

A 36.8 mg Ni metal sample, enriched to 95% in ^{62}Ni , was activated at the Karlsruhe 3.7 MV Van de Graaff accelerator using a fast-neutron beam obtained from the $^7\text{Li}(p, n)^7\text{Be}$ reaction [12, 13] at a proton energy of

*To whom correspondence should be addressed, email address: paul@vms.huji.ac.il

†Deceased

1911 keV, just above threshold. In order to ease the handling of the small sample, the metal powder was dispersed in a camphor matrix ($> 95\%$ $C_{10}H_{16}O$, 53 mg) and pressed into a pellet; after activation, the metal was recovered (36.2 mg) by subliming the camphor under vacuum. In our conditions, all neutrons are emitted in a forward cone of 120° opening angle and the angle-integrated spectrum provides a good approximation to a thermal spectrum at $kT = 25 \pm 0.5$ keV [12, 13] with an upper cut-off energy of 106 keV. Any moderation of the neutron spectrum due to the camphor matrix is negligible in the conditions of the experiment. Before each run, the accelerator was operated in pulsed mode with a repetition rate of 1 MHz and a pulse width of 10 ns. This allowed the measurement of the neutron energy spectra via TOF using a 6Li glass monitor located 1 m downstream of the 7Li target. The proton energy is verified via the cut-off energy in the spectrum. During activations, the accelerator was run in direct-current mode with beam intensities around $100 \mu A$. The time-integrated neutron flux $\langle \phi_{exp} t \rangle = (3.68 \pm 0.14) \times 10^{15} \text{ cm}^{-2}$, collected over 17.4 days, was continuously monitored by two Au foils of the same size and sandwiching the sample and determined using the experimental value $586 \pm 8 \text{ mb}$ [13] of the capture cross section of ^{197}Au for neutrons with quasi-stellar ($kT = 25$ keV) energy distribution. The 6Li glass monitor recorded the neutron yield at regular intervals and the resulting flux history was used to evaluate the corrections for decay of the Au monitors during activation (see [12] for details).

To serve later as calibration in the AMS measurement, a 321.4 mg high-purity ^{nat}Ni metal powder sample was activated for 30 s at the rabbit facility of the Soreq nuclear reactor in a thermal neutron flux. Au monitors (bare or shielded by a Cd tube), separately activated in the same conditions, yielded a Cd ratio of 10.7 ± 2.3 . After neutron irradiation, the ^{65}Ni (2.5 hrs) γ activity produced in the ^{nat}Ni sample was measured in a 100 cm^3 Ge(Li) detector at a distance of 7.7 cm in order to monitor the integrated neutron flux. The efficiency of the detector was measured, using a vial which contained 0.1413 g of a ^{152}Eu calibrated solution ($6.44 \pm 0.17 \text{ kBq}$) and reproduced very closely the geometry of the ^{nat}Ni activated sample. The efficiency was determined for the three major γ lines in ^{65}Ni decay (366.3, 1115.5 and 1481.8 keV) by fitting the yields of γ lines in the ^{152}Eu decay at 344.3, 1112.1 and 1408.0 keV, very close in energy to those of ^{65}Ni and including minor corrections for summing effects. From the measured ^{65}Ni activity (corresponding to $(4.58 \pm 0.12) \times 10^9$ (1σ) ^{65}Ni atoms produced in the activation), the thermal-neutron capture and resonance integral of ^{64}Ni ($\sigma_\gamma = 1.52 \pm 0.03 \text{ b}$ and $I_\gamma = 0.98 \pm 0.3 \text{ b}$ [14], respectively) and those of ^{62}Ni ($\sigma_\gamma = 14.2 \pm 0.3 \text{ b}$, $I_\gamma = 9.6 \pm 3.5 \text{ b}$ [7]), and the isotopic abundances of ^{nat}Ni , we determine a ratio $^{63}Ni/^{58}Ni = (7.52 \pm 0.35) \times 10^{-11}$ (1σ) in the reactor-activated ^{nat}Ni sample.

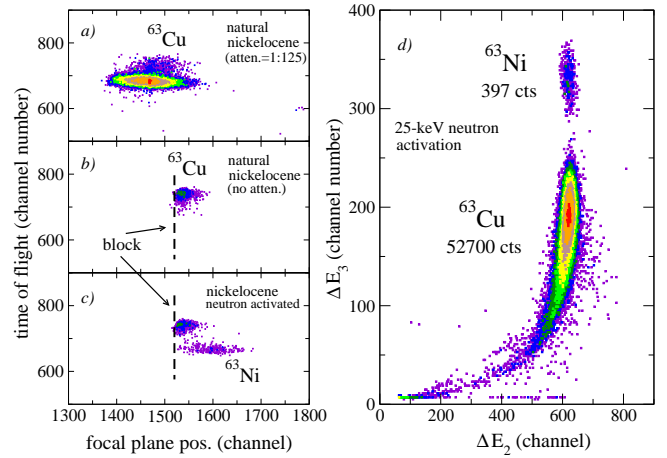


FIG. 1: Gas-filled magnet separation of the ^{63}Cu - ^{63}Ni isobaric pair : *a-c*) Two-dimensional time-of-flight vs. focal plane position spectra for: *a, b*) a ^{nat}Ni (nickelocene) sample in the ECR ion source; *c*) activated ^{nat}Ni . In *a*), the ion beam was attenuated by a factor of 125 to permit the counting of the full ^{63}Cu isobaric group. In *b*) and *c*), most of the ^{63}Cu group is blocked before the detector by a movable shield; *d*) Identification spectrum of ^{63}Ni ions in the detector blocked as in *c*), measured for the fast-neutron activated sample. The x (y) axis represents the energy loss measured in the second (third) anode of the focal-plane ionization chamber.

The AMS detection of ^{63}Ni was performed at Argonne National Laboratory, using the Electron Cyclotron Resonance (ECR) ion source [15], acceleration of $^{63}Ni^{15+}$ ions to 9.2 MeV/ u with the ATLAS facility and the gas-filled magnetic spectrograph technique [16] to separate the extremely intense stable isobaric ^{63}Cu component. A preliminary experiment [17] had shown that feeding of Ni into the ECR plasma chamber in gas phase from nickelocene ($Ni(C_5H_5)_2$) organo-metallic compound reduces the ^{63}Cu contaminant by a factor of ~ 100 compared to solid material. A similar gas-feeding technique was recently used for the detection of ^{63}Ni by AMS using a Cs-sputter negative ion source [18]. For the present experiment, both the fast-neutron and the reactor-neutron activated samples were chemically converted to nickelocene at the University of Jyväskylä [19]. In order to ensure reliable yields in the synthesis process which required Ni sample masses above $\sim 100 \text{ mg}$, the fast-neutron activated sample was mixed with 101.3 mg of high-purity ^{nat}Ni before nickelocene synthesis. The chemical synthesis (involving dissolution of the metal in HCl, reaction with NaC_5H_5 , evaporation to dryness and sublimation of $Ni(C_5H_5)_2$), ensured complete isotopic homogenization of the sample, resulting also in averaging the fast-neutron activation over the whole angular range; 244.6 mg and 668.5 mg nickelocene from the fast-neutron and reactor-activated samples respectively, were obtained. It is important to note that the efficiencies of the chemical procedure or ion production and transport do not affect

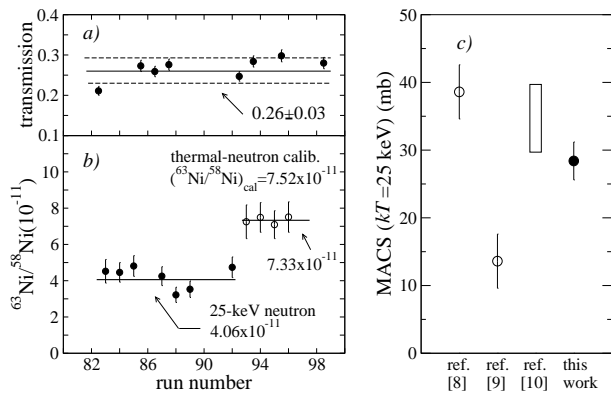


FIG. 2: *a*) Beam transmission through the accelerator during the experiment. The solid and dashed lines are the unweighted mean and standard deviation of the measured values respectively; *b*) Repeated measurements of the $^{63}\text{Ni}/^{58}\text{Ni}$ ratio for the fast-neutron activated sample (solid dots) and the calibration thermal-neutron activated sample (open dots). The error bars include (in quadrature) statistical counting error, standard deviation of the mean beam transmission (*a*) and an estimated error on the $^{58}\text{Ni}^{15+}$ mean current during each run (see text). The solid lines indicate the weighted mean of the measurements; *c*) Comparison of the present experimental value of the total Maxwellian averaged $^{62}\text{Ni}(n, \gamma)^{63}\text{Ni}$ cross section ($kT=25$ keV) (solid dot) with evaluations from [8], [9] (open dots) and of [10] (open box). The values from [8] and [9] were corrected for a thermal energy of 25 keV, using the temperature dependence of [9], in order to compare them with the experimental value.

the measurements of isotopic ratios, assuming that mass fractionation effects therein are negligible. The ATLAS accelerator system was entirely tuned with a stable beam of $^{84}\text{Kr}^{20+}$ prior to the AMS measurement of $^{63}\text{Ni}^{15+}$. The two ions have nearly equal m/q mass-to-charge ratios ($\delta(m/q)/(m/q) = 6.4 \times 10^{-5}$) and are assumed to be transported identically from the ion source to the detection system. The latter was a large hybrid detector composed of a (x, y) position-sensitive parallel-grid avalanche counter (measuring also the ion TOF relative to the accelerator RF trigger) and a multi-anode ionization chamber [20], located in the focal plane of the gas-filled Enge split-pole magnetic spectrograph. The entrance aperture of the detector ($48 \text{ cm} \times 10 \text{ cm}$) ensured 100% acceptance of the ions reaching the focal plane. The spectrograph, filled with N_2 at 20 Torr, focused the ^{63}Ni and ^{63}Cu ions into groups ~ 3 cm wide (FWHM), separated from each other by ~ 5.5 cm (Fig. 1*a-c*). This physical separation allows one to block more than 95% of the extremely intense ^{63}Cu group ($\sim 7 \times 10^4$ ions/s) and let the entire ^{63}Ni group enter into the detector for further discrimination. The latter is achieved by multiple energy-loss measurements along the ion path in the ionization chamber (Fig. 1*d*).

The beam transmission through the accelerator was repeatedly monitored (Fig. 2*a*) during the experiment be-

tween sample measurements, by injecting a small amount of isotopically enriched ^{84}Kr gas into the ion source and measuring the ion current at the injection line and before the spectrograph. The value and random error adopted for the beam transmission were the unweighted mean and standard deviation of the repeated measurements, respectively. The count rate of identified ^{63}Ni ions (Fig. 1*d*), corrected for beam transmission (Fig. 2*a*) and for a detection efficiency of 0.90 (purely systematic) due to grid shadowing, is divided by the ion current of the stable $^{58}\text{Ni}^{15+}$ beam measured after mass analysis at the accelerator injection line, to yield the $^{63}\text{Ni}^{15+}/^{58}\text{Ni}^{15+}$ isotopic ratio (Fig. 2*b*). An additional correction factor of 0.90 ± 0.04 in the $^{58}\text{Ni}^{15+}$ ion current measured in the injection line was deemed necessary for the fast-neutron activated sample, due to the near degeneracy of $^{58}\text{Ni}^{15+}$ and $^{62}\text{Ni}^{16+}$ beams. This correction was obtained by scanning the intensity of the main Ni isotopes and charge states. It is negligible in the case of the reactor-activated sample which has a very small (natural) ^{62}Ni abundance. In order to reduce unknown systematic errors in the determination of the isotopic ratios, the latter were normalized to the calibration sample (reactor-activated) by multiplying by a factor 1.03 ± 0.08 (ratio between the values obtained for the reactor-activated sample in γ and AMS measurements, see Fig. 2*b*). From the final determination in the fast-neutron activated (diluted) sample $^{63}\text{Ni}/^{58}\text{Ni} = (4.17 \pm 0.37) \times 10^{-11}$ (weighted mean and standard deviation of the mean of repeated measurements), the number of ^{58}Ni atoms in the sample and the number of ^{62}Ni atoms in the initial ^{62}Ni -enriched sample, we derive a ratio $r = ^{63}\text{Ni}/^{62}\text{Ni} = (8.78 \pm 0.79) \times 10^{-11}$.

We define the experimental capture cross section as $\sigma_{exp} = \int_0^{E_{co}} \sigma(E) \phi_{exp}(E) dE / \int_0^{E_{co}} \phi_{exp}(E) dE$, where $\phi_{exp}(E)$ denotes the experimental neutron energy spectrum and E_{co} its cut-off energy ($E_{co} = 106$ keV). σ_{exp} is related to the measured isotopic ratio r by $\sigma_{exp} = r / \int_0^{E_{co}} \int \phi_{exp}(E, t) dt dE = r / \langle \phi_{exp} t \rangle$, where we implicitly use the fact that $\phi_{exp}(E, t)$ varies only in intensity during the experiment, its energy distribution $\phi_{exp}(E)$ staying unchanged. A correction factor f_∞ must be applied to σ_{exp} to account for the $^{62}\text{Ni}(n, \gamma)$ yield at energies $E > E_{co}$. f_∞ was calculated as 1.05 ± 0.01 , using for $\sigma(E)$ expressions derived in [10] for direct capture. This mechanism was shown in [10] to be dominant, as also confirmed experimentally by the present work (see below). The $^{62}\text{Ni}(n, \gamma)^{63}\text{Ni}$ MACS at $kT = 25$ keV, $\sigma_V = \int \sigma v \phi(v) dv / v_T$, is finally given by $\sigma_V = (2/\sqrt{\pi}) f_\infty \sigma_{exp}$ [6, 13]. From our measured values, we determine $\sigma_V(^{62}\text{Ni}) = 28.4 \pm 2.8$ mb. This value is compared in Fig. 2*c*) with existing evaluations. The recent calculation of [10] including a direct-capture component is fairly consistent with the experimental value.

Figure 3 illustrates the results of stellar-evolution calculations when different values of $\sigma_V(^{62}\text{Ni})$ are used,

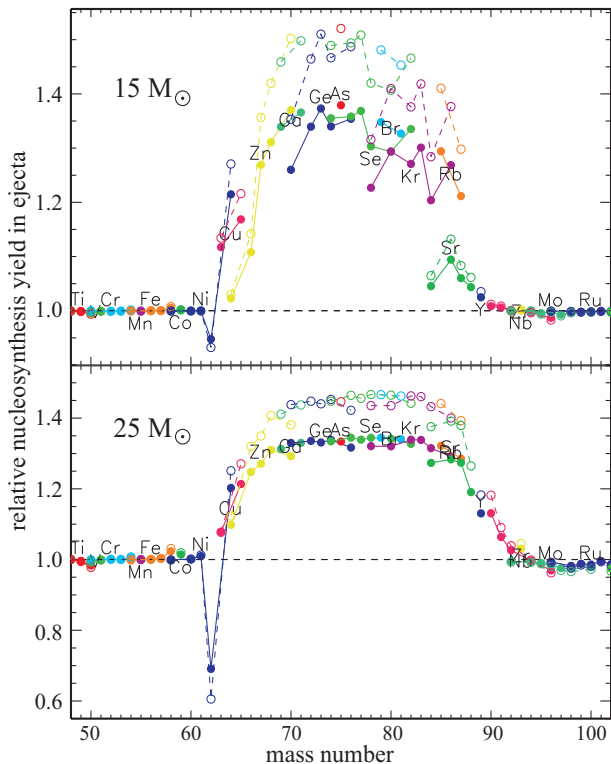


FIG. 3: Nucleosynthesis yields as function of mass number calculated for different values of the $^{62}\text{Ni}(n, \gamma)^{63}\text{Ni}$ cross section at $kT = 30$ keV and normalized to the yields at a cross section of 12.5 mb [3], for a $15 M_{\odot}$ (top) and $25 M_{\odot}$ (bottom) star. Solid dots represent the ratios between the yields calculated using 26.1 mb (this work, extrapolated from 28.4 mb at $kT = 25$ keV) to that using 12.5 mb [9]. Open dots represent the ratios between yields for 35.5 mb [8, 10] and 12.5 mb [9]. Solid (open) dots corresponding to isotopes of a given element are connected by solid (dashed) lines.

relative to the results of models S15 and S25 [3] for a $15 M_{\odot}$ and $25 M_{\odot}$ star respectively. The calculations differ solely by the value adopted for $\sigma_V(^{62}\text{Ni})$: 28.4 mb ($kT = 25$ keV; this work), 35.5 mb ($kT = 30$ keV; [8]) or 12.5 mb ($kT = 30$ keV; [3, 9]) and assume the same temperature dependence of $\sigma_V(^{62}\text{Ni})$ as in [9]. The mass region $60 < A < 90$ exhibits the characteristic abundance peak due to the weak s -process in massive stars [2]. These s -yields are strongly influenced by the change in $\sigma_V(^{62}\text{Ni})$. The increase in this cross section from 12.5 mb to the present value of 28.4 mb has two effects: (i) the overproduction of ^{62}Ni itself [3] is damped by the larger destruction probability, as indicated by the dip in Fig. 3; (ii) its effect of bottle neck in the reaction flow between the major seed nuclei ^{56}Fe , ^{58}Ni and the whole mass region $63 < A < 90$ is reduced and s -process yields are enhanced by $\sim 30\%$. The latter trend, which even amplifies the overproduction in this region compared to solar abundances, stresses that in addition to the need for a better

assessment of the rate of the neutron-producing reaction $^{22}\text{Ne}(\alpha, n)^{25}\text{Mg}$ [21], the cross section data for other potential bottle neck nuclides (e.g. ^{58}Fe , ^{60}Ni) must be verified as well.

Our direct measurement of the Maxwellian-averaged ($kT = 25$ keV) cross section of $^{62}\text{Ni}(n, \gamma)^{63}\text{Ni}$ (28.4 ± 2.8 mb) combines neutron activation with accelerator mass spectrometry, a technique which complements the traditional experiments in cases where the decay of the activation product cannot be measured. The sensitivity of nucleosynthesis calculations to individual cross sections in the non-equilibrium situation of the weak s -process, which significantly contributes to the chemical history of the universe, calls for an update of the data set of (n, γ) astrophysical rates.

This work was supported in part by the US-DOE, Office of Nuclear Physics, under Contract No. W-31-109-ENG-38 and by the USA-Israel Binational Science Foundation (BSF). A.H. and R.R. performed this work under the auspices of the U.S. Department of Energy at the Los Alamos National Laboratory operated by the University of California under contract No. W-7405-ENG-36.

-
- [1] C. Sneden and J.J. Cowan, *Science* **299**, 70 (2003).
 - [2] C.M. Raiteri *et al.*, *Astrophys. J.* **419**, 207 (1993).
 - [3] T. Rauscher *et al.*, *Astrophys. J.* **576**, 323 (2002).
 - [4] H. Beer *et al.*, *Astron. Astrophys.* **37**, 197 (1974).
 - [5] H. Beer and R.R. Spencer, *Nucl. Phys.* **A240**, 29 (1975).
 - [6] H. Beer *et al.*, *Ap. J. Sup. Ser.* **80**, 403 (1992).
 - [7] G.H.E. Sims and D.G. Juhnke, *J. Inorg. Nucl. Chem.* **32**, 2839 (1970).
 - [8] Z.Y. Bao and F. Käppeler, *At. Data Nucl. Data Tables* **36**, 411 (1987).
 - [9] Z.Y. Bao *et al.*, *At. Data Nucl. Data Tables* **76**, 70 (2000).
 - [10] T. Rauscher and K. H. Guber, *Phys. Rev. C* **66**, 028802 (2002).
 - [11] C. Tuniz *et al.*, *Accelerator Mass Spectrometry - Ultra-sensitive Analysis for Global Science*. CRC Press, ISBN 0-8493-4538-3, Boca Raton, Florida (1998).
 - [12] H. Beer and F. Käppeler, *Phys. Rev. C* **21**, 534 (1980).
 - [13] W. Ratynski and F. Käppeler, *Phys. Rev. C* **37**, 595 (1988).
 - [14] E. Gryntakis, *J. of Radioanal. Chem.* **46**, 159 (1978).
 - [15] M. Schlapp *et al.*, *Rev. Sci. Instr.* **69**, 631 (1998).
 - [16] M. Paul *et al.*, *Nucl. Instr. and Meth. A* **277**, 418 (1989).
 - [17] H. Nassar *et al.*, *Proc. 6th Int. Conf. on Radioactive Nuclear Beams*, 22-26 Sep, 2003, Argonne, Ill., USA (2003).
 - [18] T. Straume *et al.*, *Nature* **424**, 539 (2003).
 - [19] H. Koivisto *et al.*, *Nucl. Instr. and Meth. B* **94**, 291 (1994).
 - [20] M. Paul *et al.*, *Physics Division Ann. Rep.*, ANL-97/14, p. 79 (1997).
 - [21] M. Jaeger *et al.*, *Phys. Rev. Lett.* **87**, 202501 (2001).